

Orbital Lamb shift and mixing of the pseudo-zero-mode Landau levels in *ABC*-stacked trilayer graphene

K. Shizuya

*Yukawa Institute for Theoretical Physics
Kyoto University, Kyoto 606-8502, Japan*

In a magnetic field graphene trilayers support a characteristic multiplet of 12 zero(-energy)-mode Landau levels with a threefold degeneracy in Landau orbitals. It was earlier noted for bilayer graphene that Coulombic vacuum fluctuations, specific to graphene, lift the orbital degeneracy of such zero-energy modes and that these “Lamb-shifted” orbital modes, with filling, get mixed via the Coulomb interaction. It is pointed out that analogous orbital Lamb shift and mixing of zero-mode levels can also take place, with an enriched symmetry content, in *ABC*-stacked trilayer graphene; and its consequences are discussed in the light of experimental results.

PACS numbers: 73.22.Pr, 73.43.-f, 75.25.Dk

I. INTRODUCTION

Graphene,¹⁻³ an atomic layer of graphite that supports massless Dirac fermions, attracts great attention for its unique and promising electronic properties. Recently interest appears to center on bilayers and few layers of graphene, where the added layer degree of freedom makes the physics and applications of graphene richer. In particular, bilayer graphene and some types of multilayers enjoy the property that their band gaps are externally tunable.⁴⁻⁷

A notable signal of Dirac fermions is the fact that graphene, in a magnetic field, supports a characteristic set of zero-energy Landau levels, whose emergence and degeneracy have a topological origin in the chiral anomaly.⁸ Monolayer graphene has four such zero-energy levels owing to the spin and valley degeneracy, and they are responsible for the observed half-integer quantum Hall effect.^{1,2} In bilayer graphene there are eight such levels, with an extra twofold degeneracy⁴ in Landau orbitals $n=0$ and 1. This “orbital” degeneracy is a consequence of topology and the added layer, and N -layer graphene necessarily has $4N$ zero-energy Landau levels with N -fold orbital degeneracy. In the presence of Zeeman coupling, Coulomb interactions, etc., these zero-energy levels evolve into a variety of pseudo-zero-mode (PZM) levels, or broken-symmetry states, as discussed theoretically.⁹⁻¹¹ The interplay of orbital degeneracy and Coulomb interactions brings about a new realm of quantum phenomena^{9,12-16} in the PZM sector, such as orbital mixing and orbital-pseudospin waves.

Graphene is distinguished from conventional electron systems by the feature that it is an intrinsically many-body system equipped with the quantum vacuum, or the valence band acting as the Dirac sea. Quantum fluctuations of the Dirac sea are sizable, even leading to ultraviolet divergences; and one encounters such field-theoretic (or many-body) phenomena as velocity renormalization,¹⁷ screening of charge,¹⁸ and nontrivial Coulombic corrections to cyclotron resonance.¹⁹⁻²³ Quantum fluctuations also affect the PZM levels sub-

stantially. They work to lift²⁴ the orbital degeneracy of the PZM levels in bilayer graphene; each orbital mode responds to quantum fluctuations differently and gets shifted, just like the Lamb shift²⁵ in the hydrogen atom, where the field-theoretic effect of quantum electrodynamics was revealed for the first time historically. The Lamb-shifted orbital modes get mixed via Coulomb interactions and govern the fine structure of the PZM sector.

A number of recent experiments²⁶⁻³² have verified that the electronic properties of graphene trilayers strongly depend on the stacking order, with Bernal (*ABA*)-stacked trilayers remaining metallic in contrast to rhombohedral (*ABC*-stacked) trilayers which exhibit a tunable band gap. Actually trilayers drew theorists’ attention³³⁻³⁶ even before experiments and their rich electronic properties³⁷⁻³⁹ have been under active study. Currently considerable attention⁴⁰⁻⁴² is directed to *ABC*-stacked trilayers which are a chiral generalization of bilayer graphene. In view of this, it is of interest to ask how the Coulombic vacuum and orbital dynamics generalizes to trilayers.

The purpose of this paper is to examine the effect of Coulombic vacuum fluctuations in trilayers and show that the orbital Lamb shift and orbital mixing of the PZM levels are also present, with an enriched symmetry content, in *ABC*-stacked trilayer graphene. It is noted, in particular, that level mixing takes place without level crossing; this mechanism would, for high-quality samples, lead to an observable sequence of fully-split broken-symmetry quantum Hall states in the PZM sector.

In Sec. II we briefly review some basic features of the PZM levels in *ABC*-trilayer graphene, and in Sec. III show that vacuum fluctuations lift their orbital degeneracy. In Sec. IV we discuss in a simplified setting how orbital mixing of the PZM levels takes place via the Coulomb interaction. In Sec. V we examine the hierarchy of broken-symmetry states under practical conditions. Section VI is devoted to a summary and discussion.

II. TRILAYER GRAPHENE

The *ABC*-stacked trilayer graphene consists of three graphene layers with vertically-arranged dimer bonds (B_1, A_2) and (B_2, A_3), where (A_i, B_i) denote inequivalent lattice sites in the i -th layer. The interlayer coupling $\gamma_0 \equiv \gamma_{B_i A_i} \sim 3$ eV is related to the Fermi velocity $v = (\sqrt{3}/2)a_L \gamma_0 / \hbar \sim 10^6$ m/s in monolayer graphene. Interlayer hopping via the nearest-neighbor dimer coupling⁴³ $\gamma_1 \equiv \gamma_{B_1 A_2} = \gamma_{B_2 A_3} \sim 0.4$ eV leads to soft cubic spectra³³ $\propto |\mathbf{p}|^3$ in the low-energy branches $|\epsilon| < \gamma_1$.

The effective Hamiltonian for *ABC*-stacked trilayer graphene with such intralayer and interlayer couplings is written as³⁶

$$\begin{aligned} H^{\text{tri}} &= \int d^2\mathbf{x} \left[(\Psi^K)^\dagger \mathcal{H}_K \Psi^K + (\Psi^{K'})^\dagger \mathcal{H}_{K'} \Psi^{K'} \right], \\ \mathcal{H}_K &= \begin{pmatrix} D_1 & V & W \\ V^\dagger & D_2 & V \\ W^\dagger & V^\dagger & D_3 \end{pmatrix}, \\ D_i &= \begin{pmatrix} U_i & v p^\dagger \\ v p & U_i \end{pmatrix}, \quad V = \begin{pmatrix} -v_4 p^\dagger & v_3 p \\ \gamma_1 & -v_4 p^\dagger \end{pmatrix}, \\ W &= \begin{pmatrix} 0 & \gamma_2/2 \\ 0 & 0 \end{pmatrix}, \end{aligned} \quad (1)$$

with $p = p_x + ip_y$ and $p^\dagger = p_x - ip_y$. Here $\Psi^K = (\psi_{A_1}, \psi_{B_1}, \psi_{A_2}, \psi_{B_2}, \psi_{A_3}, \psi_{B_3})^\dagger$ stands for the electron field at the K valley. v_3 and v_4 are related to the non-leading interlayer couplings $\gamma_3 \equiv \gamma_{A_1 B_2}$ and $\gamma_4 \equiv \gamma_{A_1 A_2}$, respectively, and $\gamma_2 \equiv \gamma_{A_1 B_3}$. (U_1, U_2, U_3) stand for the on-site energies of the three layers; we take $U_2 = 0$ without loss of generality. As in bilayer graphene,⁴ these biases $\{U_i\}$ open a tunable band gap³³ $\sim U_1 - U_3$. \mathcal{H}_K is diagonal in (suppressed) electron spin.

The Hamiltonian $\mathcal{H}_{K'}$ at another valley is given by \mathcal{H}_K with $p \rightarrow -p_x + ip_y = -p^\dagger$ and $p^\dagger \rightarrow -p$, and acts on a spinor of the same sublattice content as Ψ^K . Actually, $\mathcal{H}_{K'}$ is unitarily equivalent to \mathcal{H}_K with the sign of v_3 and γ_2 reversed and with layer 1 and layer 3 interchanged,

$$\begin{aligned} S^\dagger \mathcal{H}_{K'} S &= \mathcal{H}_K|_{-v_3, -\gamma_2; U_1 \leftrightarrow U_3}, \\ S &= \begin{pmatrix} & & \sigma_2 \\ & -\sigma_2 & \\ \sigma_2 & & \end{pmatrix}. \end{aligned} \quad (2)$$

In view of this, we adopt $\hat{\mathcal{H}}_{K'} = S^\dagger \mathcal{H}_{K'} S$ for $\mathcal{H}_{K'}$ and simply pass to the K' valley by reversing the sign of v_3 and γ_2 and interchanging U_1 and U_3 in the K -valley expressions. Nonzero v_3 , γ_2 and bias $U_1 - U_3$ thus act as valley-symmetry breakings. Remember that in this representation $\hat{\mathcal{H}}_{K'}$ acts on a spinor of the form $\Psi^{K'} = (\psi_{B_3}, \psi_{A_3}, \psi_{B_2}, \psi_{A_2}, \psi_{B_1}, \psi_{A_1})^\dagger$.

A direct link between the K - and K' -valley representations, such as Eq. (2), was also noted²⁴ for bilayer graphene. We remark that such a link is not shared by *ABA*-stacked trilayers, where the Landau-level spectra significantly differ³⁷ between the two valleys for nonzero biases (though they coincide for zero bias).

We have discussed the general structure of trilayer parameters for completeness. For our present analysis of quantum effects in *ABC* trilayers we retain only the leading parameters (v, γ_1, U_i); the effect of nonleading couplings (v_3, v_4, γ_2) is discussed later in Sec. V. In addition, we focus on the case of a symmetric bias³³ by choosing $U_3 = -U_1 \equiv u/2$.

Let us place trilayer graphene in a strong uniform magnetic field $B_z = B > 0$ normal to the sample plane; we set, in \mathcal{H}_K , $p \rightarrow \Pi = p + eA$ with $A = A_x + iA_y = -By$, and denote the magnetic length as $\ell = 1/\sqrt{eB}$; setting $a \equiv \sqrt{2eB} \Pi^\dagger$ then yields $[a, a^\dagger] = 1$. It is easily seen that the eigenmodes of \mathcal{H}_K have the structure

$$\begin{aligned} \Psi_n &= \left(|n-3\rangle b_n^{(1)}, |n-2\rangle d_n^{(1)}, |n-2\rangle b_n^{(2)}, \right. \\ &\quad \left. |n-1\rangle d_n^{(2)}, |n-1\rangle b_n^{(3)}, |n\rangle d_n^{(3)} \right)^\dagger \end{aligned} \quad (3)$$

with $n = 0, 1, 2, \dots$, where only the orbital eigenmodes are shown using the standard harmonic-oscillator basis $\{|n\rangle\}$ (with the understanding that $|n\rangle = 0$ for $n < 0$). The coefficients $\mathbf{v}_n = (b_n^{(1)}, d_n^{(1)}, b_n^{(2)}, d_n^{(2)}, b_n^{(3)}, d_n^{(3)})^\dagger$ for each $n = 3, 4, \dots$ are given by the eigenvectors (chosen to form an orthonormal basis) of the reduced Hamiltonian $\hat{\mathcal{H}}_{\text{red}} \equiv \omega_c \mathcal{H}_n$ with

$$\mathcal{H}_n = \begin{pmatrix} -M & \sqrt{n-2} & & & & \\ \sqrt{n-2} & -M & & & & \\ & & \hat{\gamma} & & & \\ & & \hat{\gamma} & 0 & \sqrt{n-1} & \\ & & & \sqrt{n-1} & 0 & \hat{\gamma} \\ & & & & \hat{\gamma} & M & \sqrt{n} \\ & & & & & \sqrt{n} & M \end{pmatrix}, \quad (4)$$

where

$$\omega_c \equiv \sqrt{2} v / \ell \approx 36.3 \times v [10^6 \text{ m/s}] \sqrt{B [\text{T}]} \text{ meV}, \quad (5)$$

with v in units of 10^6 m/s and B in tesla, is the characteristic cyclotron energy for monolayer graphene; $M \equiv \frac{1}{2} u / \omega_c$ and $\hat{\gamma} \equiv \gamma_1 / \omega_c$. Note that eigenvectors \mathbf{v}_n can be taken real since \mathcal{H}_n is a real symmetric matrix.

Solving the secular equation shows that there are 6 branches of Landau levels for each integer $n \geq 3$. We denote the eigenvalues as $\epsilon_{-n''} < \epsilon_{-n'} < \epsilon_{-n} < 0 < \epsilon_n < \epsilon_{n'} < \epsilon_{n''}$, so that the index $\pm n$ reflects the sign of ϵ_n ; $|\epsilon_{\pm n'}| \gtrsim \gamma_1$ and $|\epsilon_{\pm n''}| \gtrsim \gamma_1$. The $|n| = 3$ levels, e.g., consist of the $n = (\pm 3, \pm 3', \pm 3'')$ branches.

There are also solutions for $n = 2, 1$ and 0 , for which \mathcal{H}_n is reduced to a matrix of smaller rank 5, 3 and 1. For $n = 0$, $\hat{\mathcal{H}}_{\text{red}}$ has an obvious eigenvalue $\epsilon_0 = U_3 = u/2$ with eigenvector $\mathbf{v}_0 = (0, 0, 0, 0, 0, 1)^\dagger$ or

$$\Psi_0 = (0, 0, 0, 0, 0, |0\rangle)^\dagger. \quad (6)$$

For $n = 1$, $\hat{\mathcal{H}}_{\text{red}}$ has three eigenvalues ($\epsilon_1, \epsilon_{\pm 1'}$), which, for $u = 0$, read $(0, \pm \sqrt{\hat{\gamma}^2 + 1}) \omega_c$. The zero-energy solution, in particular, takes the form:

$$\Psi_1 \stackrel{u=0}{=} c_1 (0, 0, 0, -\kappa |0\rangle, 0, |1\rangle)^\dagger, \quad (7)$$

with $\kappa \equiv 1/\hat{\gamma}$ and $c_1 = \hat{\gamma}/\sqrt{\hat{\gamma}^2 + 1} = 1/\sqrt{1 + \kappa^2}$. For $n = 2$, \mathcal{H}_{red} has five eigenvalues ($\epsilon_2, \epsilon_{\pm 2'}, \epsilon_{\pm 2''}$), with $\epsilon_2 = 0$ and $|\epsilon_{\pm 2'}| \sim |\epsilon_{\pm 2''}| \sim \gamma_1$ for $u = 0$. The zero-energy solution takes the form

$$\Psi_2 \stackrel{u=0}{=} c_2 (0, \sqrt{2}\kappa^2 |0\rangle, 0, -\sqrt{2}\kappa |1\rangle, 0, |2\rangle)^t, \quad (8)$$

with $c_2 = \hat{\gamma}^2/\sqrt{2 + 2\hat{\gamma}^2 + \hat{\gamma}^4} = 1/\sqrt{1 + 2\kappa^2 + 2\kappa^4}$. Note that these zero-energy solutions (Ψ_0, Ψ_1, Ψ_2) reside predominantly on the B_3 lattice sites of the third layer; correspondingly, the zero-energy solutions at the K' valley reside predominantly on the A_1 sites of the first layer.

Of our particular concern are these three zero-energy modes (Ψ_0, Ψ_1, Ψ_2). For $u = 0$ there are 12 such zero-energy Landau levels differing in spin, valley and orbital [$n = (0, 1, 2)$] degrees of freedom; their presence is dictated by the nonzero index^{8,18} of the Dirac Hamiltonian $\mathcal{H}_K \oplus \mathcal{H}_{K'}$ with only v and γ_1 retained.

For nonzero bias $u \neq 0$ they evolve into the pseudo-zero modes with nonzero energies,

$$\begin{aligned} (\epsilon_0^u, \epsilon_1^u, \epsilon_2^u) &= (1, 1 - z_1, 1 - z_2) u/2, \\ z_1 &= \kappa^2(c_1)^2 + O(\hat{u}^2\kappa^6), \\ z_2 &= 2\kappa^2(1 + 2\kappa^2)(c_2)^2 + O(\hat{u}^2\kappa^4), \end{aligned} \quad (9)$$

where $\hat{u} \equiv u/\omega_c$. One can also write $\epsilon_1^u \approx (c_1)^2 u/2$ and $\epsilon_2^u \approx (1 - 2\kappa^4)(c_2)^2 u/2$.

For a numerical estimate let us take, as typical values,⁴³ $\gamma_0 = 3.16$ eV (or $v \approx 1.0 \times 10^6$ m/s) and $\gamma_1 = 0.4$ eV. They yield $\hat{\gamma} \approx 3.41$ and $\kappa \approx 0.293$ at $B = 10\text{T}$, which in turn lead to $c_1 \approx 0.960$, $c_2 \approx 0.918$, $z_1 \approx 0.08$ and $z_2 \approx 0.17$. One thus has

$$(\epsilon_0^u, \epsilon_1^u, \epsilon_2^u) \approx (1, 0.92, 0.83) u/2 \quad (10)$$

for $u \ll \omega_c$.

One can pass to the K' valley by setting $u \rightarrow -u$ in the K -valley expressions. The eigensystems (ϵ_n, \mathbf{v}_n) at the two valleys are related as

$$\begin{aligned} \epsilon_n|_{K'} &= -\epsilon_{-n}|_K, \\ b_n^{(i)}|_{K'} &= -b_{-n}^{(i)}|_K, \quad d_n^{(i)}|_{K'} = d_{-n}^{(i)}|_K \end{aligned} \quad (11)$$

for each mode (n, n', n'') and $i \in (1, 2, 3)$. For later convenience, we continue to use $n = (0, 1, 2)$ to specify the PZM levels at the K' valley; one can thus effectively set $n = \pm 0 \rightarrow 0$, $\pm 1 \rightarrow 1$ and $\pm 2 \rightarrow 2$. When the interlayer bias u is turned on, these PZM levels go up or down oppositely at the two valleys, opening a band gap $\sim u$.

The Landau-level structure is made explicit by passing to the $|n, y_0\rangle$ basis (with $y_0 \equiv \ell^2 p_x$) via the expansion $(\Psi^K(\mathbf{x}), \Psi^{K'}(\mathbf{x})) = \sum_{n, y_0} \langle \mathbf{x} | n, y_0 \rangle \{ \psi_\alpha^{n;a}(y_0) \}$, where n refers to the level index, $\alpha \in (\uparrow, \downarrow)$ to the spin, and $a \in (K, K')$ to the valley. The charge density $\rho_{-\mathbf{p}} = \int d^2\mathbf{x} e^{i\mathbf{p}\cdot\mathbf{x}} \rho$ with $\rho = (\Psi^K)^\dagger \Psi^K + (\Psi^{K'})^\dagger \Psi^{K'}$ is thereby written as²⁴

$$\rho_{-\mathbf{p}} = \gamma_{\mathbf{p}} \sum_{k, n=-\infty}^{\infty} \sum_{\alpha, \alpha'} g_{\mathbf{p}}^{kn; \alpha} R_{\alpha\alpha'; \mathbf{p}}^{kn; \alpha\alpha'}$$

$$R_{\alpha\beta; \mathbf{p}}^{kn; ab} \equiv \int dy_0 \psi_\alpha^{k, a \dagger}(y_0) e^{i\mathbf{p}\cdot\mathbf{r}} \psi_\beta^{n, b}(y_0), \quad (12)$$

where $\gamma_{\mathbf{p}} \equiv e^{-\ell^2 \mathbf{p}^2/4}$; $\mathbf{r} = (i\ell^2 \partial/\partial y_0, y_0)$ stands for the center coordinate with uncertainty $[r_x, r_y] = i\ell^2$; the level sum \sum_n is taken over possible (n, n', n'') .

The coefficient matrix $g_{\mathbf{p}}^{kn; a} \equiv g_{\mathbf{p}}^{kn}|_a$ at valley $a \in (K, K')$ is constructed from the eigenvectors $\mathbf{v}_n|_a$,

$$\begin{aligned} g_{\mathbf{p}}^{kn} &= b_k^{(1)} b_n^{(1)} f_{\mathbf{p}}^{|k|-3, |n|-3} \\ &+ (d_k^{(1)} d_n^{(1)} + b_k^{(2)} b_n^{(2)}) f_{\mathbf{p}}^{|k|-2, |n|-2} \\ &+ (d_k^{(2)} d_n^{(2)} + b_k^{(3)} b_n^{(3)}) f_{\mathbf{p}}^{|k|-1, |n|-1} \\ &+ d_k^{(3)} d_n^{(3)} f_{\mathbf{p}}^{|k|, |n|}, \end{aligned} \quad (13)$$

where

$$f_{\mathbf{p}}^{kn} = \sqrt{n!/k!} (-\bar{q}/\sqrt{2})^{k-n} L_n^{(k-n)}(|\bar{q}|^2/2) \quad (14)$$

for $k \geq n \geq 0$, and $f_{\mathbf{p}}^{nk} = (f_{-\mathbf{p}}^{kn})^\dagger$; $\bar{q} = \ell(p_x - i p_y)$; it is understood that $f_{\mathbf{p}}^{kn} = 0$ for $k < 0$ or $n < 0$. As seen from Eq. (11), $g_{\mathbf{p}}^{kn; a}$ at the two valleys are related as

$$g_{\mathbf{p}}^{mn}|_{K'} = g_{\mathbf{p}}^{-m, -n}|_K, \quad g_{\mathbf{p}}^{mn; a}|_u = g_{\mathbf{p}}^{-m, -n; a}|_{-u}. \quad (15)$$

Within the $n \in (0, 1, 2)$ sector, $g_{\mathbf{p}}^{kn; a}$ are functions⁴⁴ of (\hat{u}^2, κ^2) and are thus common to both valleys; for $u = 0$, they read

$$\begin{aligned} g_{\mathbf{p}}^{00} &= 1, \quad g_{\mathbf{p}}^{01} = c_1 \ell p / \sqrt{2}, \quad g_{\mathbf{p}}^{10} = -c_1 \ell \bar{p} / \sqrt{2}, \\ g_{\mathbf{p}}^{02} &= c_2 \ell^2 p^2 / (2\sqrt{2}), \\ g_{\mathbf{p}}^{11} &= 1 - (c_1)^2 \frac{1}{2} \ell^2 \mathbf{p}^2, \quad g_{\mathbf{p}}^{12} = \lambda_{\mathbf{p}} g_{\mathbf{p}}^{01}, \\ g_{\mathbf{p}}^{22} &= 1 - (c_2)^2 [(1 + \kappa^2) \ell^2 \mathbf{p}^2 - \frac{1}{8} (\ell^2 \mathbf{p}^2)^2], \\ \lambda_{\mathbf{p}} &= \sqrt{2} (1 + \kappa^2 - \frac{1}{4} \ell^2 \mathbf{p}^2) c_2, \end{aligned} \quad (16)$$

with $c_1 = 1/\sqrt{1 + \kappa^2}$ and $c_2 = 1/\sqrt{1 + 2\kappa^2 + 2\kappa^4}$.

From now on we frequently suppress summations over levels n , spins α and valleys a , with the convention that the sum is taken over repeated indices. The Hamiltonian H^{bi} projected to the PZM levels is thereby written as

$$H_u = \epsilon_n^u \delta R_{\beta\beta; \mathbf{0}}^{nn} - \mu_Z (T_3)_{\beta\alpha} R_{\alpha\beta; \mathbf{0}}^{nn; aa} \quad (17)$$

with $n \in (0, 1, 2)$ and $\delta R_{\alpha\beta; \mathbf{0}}^{mn} \equiv R_{\alpha\beta; \mathbf{0}}^{mn; KK} - R_{\alpha\beta; \mathbf{0}}^{mn; K'K'}$. Here the Zeeman term $\mu_Z \equiv g^* \mu_B B \approx 0.12 B[\text{T}]$ meV is introduced via the spin matrix $T_3 = \sigma_3/2$.

III. VACUUM FLUCTUATIONS

In this section we examine the effect of Coulombic quantum fluctuations on the PZM multiplet. The Coulomb interaction is written as

$$V = \frac{1}{2} \sum_{\mathbf{p}} v_{\mathbf{p}} : \rho_{-\mathbf{p}} \rho_{\mathbf{p}} :, \quad (18)$$

where $v_{\mathbf{p}} = 2\pi\alpha/(\epsilon_b|\mathbf{p}|)$ with $\alpha = e^2/(4\pi\epsilon_0) \approx 1/137$ and the substrate dielectric constant ϵ_b ; $\sum_{\mathbf{p}} = \int d^2\mathbf{p}/(2\pi)^2$. For simplicity we ignore the difference between the intralayer and interlayer Coulomb potentials.

In this paper we generally focus on many-body ground states $|G\rangle$ with a homogeneous density, realized at integer filling factor $\nu \in [-6, 6]$. We set the expectation values $\langle G|R_{\alpha\beta;\mathbf{k}}^{mn;ab}|G\rangle = \delta_{\mathbf{k},\mathbf{0}}\rho_0\nu_{\alpha\beta}^{mn;ab}$ with $\rho_0 = 1/(2\pi\ell^2)$ and $\delta_{\mathbf{k},\mathbf{0}} = (2\pi)^2\delta^2(\mathbf{k})$; accordingly, the filling factor $\nu_{\alpha\beta}^{mn;aa} = 1$ for a filled level specified by (n, a, α) .

Let us define the Dirac sea $|\text{DS}\rangle$ as the valence band with levels below the PZM sector (i.e., levels with $n \leq -3$, $n' \leq -1'$ and $n'' \leq -2''$) all filled. We construct the Hartree-Fock Hamiltonian V^{HF} out of V as the effective Hamiltonian that governs the electron states over $|\text{DS}\rangle$. Let us write $V^{\text{HF}} = V_{\text{D}} + V_{\text{X}}$. As usual, the direct interaction $V_{\text{D}} \propto v_{\mathbf{p}\rightarrow\mathbf{0}}R_{\beta\beta;\mathbf{0}}^{m'm';bb}$ is removed if one takes into account neutralizing positive background charges. We thus focus on the exchange interaction

$$V_{\text{X}} = - \sum_{\mathbf{p}} v_{\mathbf{p}}\gamma_{\mathbf{p}}^2 g_{-\mathbf{p}}^{mn';b} g_{\mathbf{p}}^{m'n;a} \nu_{\beta\alpha}^{mn;ba} R_{\alpha\beta;\mathbf{0}}^{m'n';ab}, \quad (19)$$

where we sum over filled levels (m, n) and retain the PZM sector $m', n' \in (0, 1, 2)$.

Let us first extract, out of V_{X} , the contribution from the Dirac sea,

$$V_{\text{X}}^{\text{DS}} = - \sum_{\mathbf{p}} v_{\mathbf{p}}\gamma_{\mathbf{p}}^2 \sum_{n \in \text{DS}} |g_{\mathbf{p}}^{m'n;a}|^2 R_{\alpha\alpha;\mathbf{0}}^{m'm';aa}, \quad (20)$$

where the sum over $m' \in (0, 1, 2)$, $a \in (K, K')$ and $\alpha \in (\uparrow, \downarrow)$ is understood. Actually, the sum over infinitely many filled levels with $-\infty < n \in \text{DS}$ gives rise to an ultraviolet divergence.

Fortunately one can isolate the divergence and even evaluate V_{X}^{DS} exactly for zero bias $u \rightarrow 0$, as done for the bilayer case.²⁴ Note first that, as seen from Eq. (15), $g_{\mathbf{p}}^{mn}|_K = g_{\mathbf{p}}^{mn}|_{K'} = g_{\mathbf{p}}^{-m,-n}$ for $u = 0$, and use the completeness relation²⁴

$$\sum_{n=-\infty}^{\infty} |g_{\mathbf{p}}^{mn}|^2 = e^{\ell^2\mathbf{p}^2/2} \quad (21)$$

to extend the sum $\sum_{n \in \text{DS}}$ to its complement $\sum_{n \in \overline{\text{DS}}}$ as well. The result is

$$\sum_{n \in \text{DS}} |g_{\mathbf{p}}^{jn}|^2 \stackrel{u=0}{=} \frac{1}{2} (e^{\ell^2\mathbf{p}^2/2} - |g_{\mathbf{p}}^{j0}|^2 - |g_{\mathbf{p}}^{j1}|^2 - |g_{\mathbf{p}}^{j2}|^2), \quad (22)$$

for $j \in (0, 1, 2)$. Equation (21) was noted earlier with a formal proof; a direct proof of it is given in Appendix A. The $e^{\ell^2\mathbf{p}^2/2}$ term in Eq. (22), though leading to a divergence upon integration over \mathbf{p} , is common to all levels j and is safely omitted. We thus take the rest as the regularized expression for $\sum_{n \in \text{DS}} |g_{\mathbf{p}}^{jn}|^2$.

The regularized Dirac-sea contribution thus reads

$$V_{\text{X}}^{\text{DS}} \stackrel{u \rightarrow 0}{=} \epsilon_0^{\nu} R_{\alpha\alpha;\mathbf{0}}^{00;aa} + \epsilon_1^{\nu} R_{\alpha\alpha;\mathbf{0}}^{11;aa} + \epsilon_2^{\nu} R_{\alpha\alpha;\mathbf{0}}^{22;aa}, \quad (23)$$

$$\epsilon_j^{\nu} = \frac{1}{2} \sum_{\mathbf{p}} v_{\mathbf{p}}\gamma_{\mathbf{p}}^2 \sum_{n=0}^2 |g_{\mathbf{p}}^{jn}|^2. \quad (24)$$

Integration over \mathbf{p} , with the aid of the formula

$$\sum_{\mathbf{p}} v_{\mathbf{p}}\gamma_{\mathbf{p}}^2 [1, q^2, q^4, q^6, q^8] = [1, 1, 3, 15, 105] \tilde{V}_c \quad (25)$$

with $q \equiv \ell|\mathbf{p}|$, then yields

$$\begin{aligned} \epsilon_0^{\nu} &= \frac{1}{2} [1 + c_1^2 c_2^2 (\frac{7}{8} + \frac{11}{8} \kappa^2 + \kappa^4)] \tilde{V}_c, \\ \epsilon_1^{\nu} &= \frac{1}{2} [1 + c_1^4 c_2^2 (\frac{11}{16} + \frac{15}{16} \kappa^2 + \kappa^4)] \tilde{V}_c, \\ \epsilon_2^{\nu} &= \frac{1}{2} [1 + c_1^2 c_2^4 (\frac{29}{64} - \frac{7}{64} \kappa^2 - \frac{11}{8} \kappa^4 - \frac{15}{4} \kappa^6 - 2\kappa^8)] \tilde{V}_c, \end{aligned} \quad (26)$$

where $c_1^2 \equiv (c_1)^2$, etc., $\tilde{V}_c \equiv \sqrt{\pi/2} V_c$ and

$$V_c \equiv \alpha/(\epsilon_b \ell) \approx (56.1/\epsilon_b) \sqrt{B[\text{T}]} \text{ meV}. \quad (27)$$

Numerically,

$$(\epsilon_0^{\nu}, \epsilon_1^{\nu}, \epsilon_2^{\nu}) = (0.888, 0.777, 0.641) \tilde{V}_c \quad (28)$$

for $\hat{\gamma} = 1/\kappa \approx 3.41$ at $B = 10$ T.

Vacuum fluctuations thus shift the $n = 0, 1$ and 2 modes differently and the splitting among $(\epsilon_0^{\nu}, \epsilon_1^{\nu}, \epsilon_2^{\nu})$ reflects the difference in their spatial distributions, as is clear from Eq. (24). The empty PZM levels are ordered as $\epsilon_0^{\nu} > \epsilon_1^{\nu} > \epsilon_2^{\nu} > 0$. Actually the spectra vary with filling of the PZM sector. Note Eq. (20), which tells us to include extra contributions $-|g^{jn}|^2$ for ϵ_j^{ν} , when the $n \in (0, 1, 2)$ level is filled. In particular, when the PZM sector is filled up, one finds that $\{\epsilon_j^{\nu}\}$ change sign so that they are ordered as $\epsilon_0^{\nu} < \epsilon_1^{\nu} < \epsilon_2^{\nu} < 0$.

Let us next suppose filling the lowest-lying $n = 2$ level first in the empty PZM sector (for $u = \mu_Z = 0$). One then finds $\epsilon_2^{\nu} \approx 0.054 \tilde{V}_c$ for $g \approx 3.41$. If, instead, the highest-lying $n = 0$ level were first filled, one would find $\epsilon_0^{\nu} \approx -0.11 \tilde{V}_c$. This puzzling situation suggests that one cannot reach the true ground state by filling the $n = 2$ level alone. It is clear now that one has to diagonalize the exchange interaction (19), with mixing among the $n = (0, 1, 2)$ orbital modes taken into account.

IV. MIXING OF THE PZM LEVELS

In this section we examine how the PZM sector changes in spectrum with filling. The first step is to extract from V_{X} in Eq. (19) the exchange interaction acting within the $n = (0, 1, 2)$ sector,

$$\begin{aligned} V_{\text{X}}^{\text{PZ}} &= - \sum_{\mathbf{p}} v_{\mathbf{p}}\gamma_{\mathbf{p}}^2 \Gamma_{\mathbf{p}}^{nm} R_{\mathbf{0}}^{mn}, \\ \Gamma_{\mathbf{p}}^{00} &= \nu^{nn} |g_{\mathbf{p}}^{n0}|^2, \Gamma_{\mathbf{p}}^{11} = \nu^{nn} |g_{\mathbf{p}}^{n1}|^2, \Gamma_{\mathbf{p}}^{22} = \nu^{nn} |g_{\mathbf{p}}^{n2}|^2, \\ \Gamma_{\mathbf{p}}^{10} &= g_{\mathbf{p}}^{00} g_{-\mathbf{p}}^{11} \nu^{10} + g_{\mathbf{p}}^{01} g_{-\mathbf{p}}^{21} \nu^{21}, \\ \Gamma_{\mathbf{p}}^{21} &= g_{\mathbf{p}}^{10} g_{-\mathbf{p}}^{12} \nu^{10} + g_{\mathbf{p}}^{11} g_{-\mathbf{p}}^{22} \nu^{21}, \\ \Gamma_{\mathbf{p}}^{20} &= g_{\mathbf{p}}^{00} g_{-\mathbf{p}}^{22} \nu^{20}, \end{aligned} \quad (29)$$

where $m, n \in (0, 1, 2)$; $\Gamma_{\mathbf{p}}^{01} \equiv (\Gamma_{-\mathbf{p}}^{10})^*$, $\Gamma_{\mathbf{p}}^{21} \equiv (\Gamma_{-\mathbf{p}}^{12})^*$, etc. For conciseness the spin and valley indices have been suppressed in the above; $\nu^{nn} R_{\mathbf{0}}^{00}$, e.g., reads $\nu_{\beta\alpha}^{nn;ba} R_{\alpha\beta;0}^{00;ab}$.

Let us, for the moment, freeze the spin and valley degrees of freedom and focus on the orbital degrees of freedom. The PZM sector then consists of three levels $n \in (0, 1, 2)$ governed by the effective Hamiltonian $\mathcal{V} \equiv V_X^{\text{DS}} + V_X^{\text{PZ}} = H^{mn} R_{\mathbf{0}}^{mn}$ with $H^{mn} = \epsilon_n^v \delta^{mn} - \sum_{\mathbf{p}} v_{\mathbf{p}} \gamma_{\mathbf{p}}^m \Gamma_{\mathbf{p}}^{mn}$. Note that $\Gamma_{\mathbf{p}}^{mn}$ are real for real filling factors ν^{mn} , which we take. It therefore suffices to use a real $O(3)$ rotation, rather than a full $SU(3)$ rotation, to diagonalize the 3×3 real symmetric matrix H^{mn} . We thus rotate $\psi^m = (\psi^0, \psi^1, \psi^2)$ in orbital space,

$$\psi^m(y_0) = [\mathcal{U}(\theta_2, \theta_1, \theta_0)]^{mn} \Phi^n(y_0), \quad (30)$$

with three Euler angles $(\theta_2, \theta_1, \theta_0)$ parameterizing

$$\mathcal{U}(\theta_2, \theta_1, \theta_0) = e^{i\theta_2 t_2} e^{i\theta_1 t_1} e^{i\theta_0 t_0}, \quad (31)$$

where the spin-1 generators $(t_a)^{bc} \equiv i\epsilon^{bac}$ in terms of the totally antisymmetric tensor ϵ^{abc} with $\epsilon^{012} = 1$. Note that θ_0 mixes $n = (1, 2)$, θ_1 mixes $(0, 2)$, etc.

Via the rotation, $\mathcal{V} = H^{mn} R_{\mathbf{0}}^{mn} = \mathcal{H}^{mn} \mathcal{R}_{\mathbf{0}}^{mn}$ with $\mathcal{H} = \mathcal{U}^\dagger H \mathcal{U}$, where $\mathcal{R}_{\mathbf{0}}^{mn}$ stand for the charge operators for Φ^n , i.e., $R_{\alpha\beta;0}^{mn;ab}$ with $\psi_{\beta}^{n;b} \rightarrow \Phi_{\beta}^{n;b}$. The transformed fields Φ^n are taken to diagonalize \mathcal{H}^{mn} and hence the associated filling factors as well, $N_n \propto \langle G | (\Phi^n)^\dagger \Phi^n | G \rangle$ with $0 \leq N_n \leq 1$ and $n \in (0, 1, 2)$; one can now write $\nu^{mn} = (U_{mn'})^* N_{n'} (U^t)_{n'n}$.

Let us start filling the empty PZM sector at (relative) filling factor $n_f = 0$. Obviously, in view of level splitting (28), it is the lowest-lying $n = 2$ level (Φ^2) that starts to be filled. To follow how it evolves let us suppose that it is filled with fraction $n_f \leq 1$ and substitute $(N_0, N_1, N_2) = (0, 0, n_f)$. \mathcal{H}^{mn} is diagonalized if one can adjust $(\theta_0, \theta_1, \theta_2)$ so that $\mathcal{H}^{01} = \mathcal{H}^{02} = \mathcal{H}^{12} = 0$.

Note first that, with no level mixing, i.e., $\theta_0 = \theta_1 = \theta_2 = 0$, the eigenvalues $\{\mathcal{H}^{mn}\}$ simply go down with increasing n_f . Note next that, to first order in $\{\theta_n\}$,

$$\begin{aligned} \mathcal{H}^{12} &\approx (0.136 - 0.268 n_f) \theta_0 + \dots, \\ \mathcal{H}^{02} &\approx -(0.247 - 0.130 n_f) \theta_1 + \dots, \\ \mathcal{H}^{01} &\approx -0.201 n_f \theta_0 + (0.111 + 0.0626 n_f) \theta_2 + \dots \end{aligned} \quad (32)$$

This structure reveals that $\theta_0 = \theta_1 = \theta_2 = 0$ for $n_f < n_{\text{cr}} \approx 0.507$ while $\theta_0 \neq 0$ is possible for $n_f > n_{\text{cr}}$. Solving for $\{\theta_n\}$ numerically for $n_f \geq n_{\text{cr}}$ shows that the energy eigenvalue \mathcal{H}^{22} is indeed lowered for $n_f > n_{\text{cr}}$ with $\theta_0 \neq 0$. One can then reach the $n_f = 1$ state, and setting $(N_0, N_1, N_2) \rightarrow (0, n_f - 1, 1)$, etc., takes one further to the $n_f = 2$ and 3 states.

Figure 1 (a) shows how angles $\{\theta_n\}$ vary as n_f is increased from 0 to 3. Actually we find another solution which differs from one shown in the figure by signs, $(\theta_2, \theta_1, \theta_0) \rightarrow (-\theta_2, \theta_1, -\theta_0)$. These two solutions are related by a unitary transformation $Y = \text{diag}[-1, 1, -1]$, with $\mathcal{U}(-\theta_2, \theta_1, -\theta_0) = Y \mathcal{U}(\theta_2, \theta_1, \theta_0) Y^{-1}$, so that $Y \psi =$

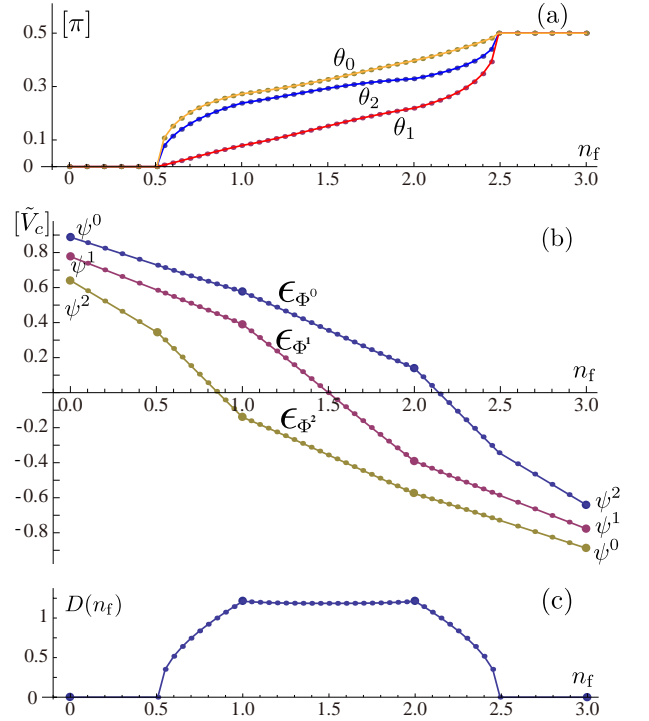


FIG. 1: Orbital mixing. (a) Angles $(\theta_0, \theta_1, \theta_2)$ vary from 0 to $\pi/2$ with filling of the (Φ^0, Φ^1, Φ^2) sector. (b) Variations of the spectra of the Φ^0, Φ^1 and Φ^2 levels over the range of relative filling factor $n_f \in [0, 3]$. (c) Electric dipole moment induced via orbital mixing.

$\mathcal{U}(-\theta_2, \theta_1, -\theta_0) Y \Phi$. They naturally lead to the same level spectra $\{\epsilon_{\Phi^n}\}$ depicted in Fig. 1 (b).

In Fig. 1 (a), each θ_n evolves from 0 to $\pi/2$ with increasing n_f . The eigenmodes (Φ^0, Φ^1, Φ^2) thereby continuously change from (ψ^0, ψ^1, ψ^2) to $(\psi^2, -\psi^1, \psi^0)$. The empty $n = (0, 1, 2)$ levels at $n_f = 0$ thus turn into the filled $n = (2, 1, 0)$ levels of energies $(-|\epsilon_2^v|, -|\epsilon_1^v|, -|\epsilon_0^v|)$, respectively, at $n_f = 3$, without any level crossing. Each spectrum $\epsilon_{\Phi^n}(n_f)$ goes down with n_f , with marked change across $n_f \sim (0.51, 1, 2, 2.49)$. The spectra as a whole realize particle-hole symmetry, with $\epsilon_{\Phi^0}(n_f) = -\epsilon_{\Phi^2}(3 - n_f)$ and $\epsilon_{\Phi^1}(n_f) = -\epsilon_{\Phi^1}(3 - n_f)$ in obvious notation. In particular, the band gaps at $n_f = 1$ and 2 are equal, with

$$\epsilon^{\text{gap}}|_{n_f=1,2} \approx 0.53 \tilde{V}_c, \quad (33)$$

considerably smaller than the full Coulombic gap $2\epsilon_2^v \approx 1.28 \tilde{V}_c$.

A special feature associated with orbital mixing is that charge carriers acquire electric dipole moment, as noted earlier^{12,14} for bilayer graphene. To see this let us consider coupling to an external scalar potential A_0 , with the Hamiltonian $H_A = -e \sum_{\mathbf{p}} (A_0)_{\mathbf{p}} \rho_{-\mathbf{p}}$. Note that $g_{\mathbf{p}}^{01}, g_{\mathbf{p}}^{12}$ (in $\rho_{-\mathbf{p}} \propto p$), which implies that orbital mixing gives rise to coupling to an inplane electric field $\mathbf{E}_{\parallel} = (E_x, E_y) = -\nabla A_0$. Indeed, for a spatially almost uniform field \mathbf{E}_{\parallel} , the relevant portion of H_A is written as

$H_A \approx h_A^{mn} R_0^{mn}$ with $h_A = -c_2 (e\ell/\sqrt{2}) (E_y T_y + E_x T_x)$, where

$$T_y = \begin{pmatrix} & 1 & \\ 1 & & \lambda \end{pmatrix}, T_x = i \begin{pmatrix} & -1 & \\ 1 & & -\lambda \end{pmatrix} \quad (34)$$

act on fields $(\psi^0, \psi^1, \psi^2)^t$ and $\lambda \equiv \lambda_{\mathbf{p}=0} = \sqrt{2} (1 + \kappa^2) c_2$.

The expectation value $\langle G|H_A|G \rangle$ then reads

$$\langle G|H_A|G \rangle \approx \rho_0 \int d^2\mathbf{x} (-\mathbf{d} \cdot \mathbf{E}_{\parallel}), \quad (35)$$

where $\mathbf{d} = (0, d_y)$ and $d_y = (e\ell/\sqrt{2}) c_1 D(n_f)$ with function $D(n_f) \equiv (T_y + \lambda T_x)^{mn} \nu^{mn}$ given by the plot in Fig 1 (c). This shows that electrons acquire electric dipole moment of magnitude $|\mathbf{d}_e| = (e\ell/\sqrt{2}) c_1 |D(n_{pz})|$ (per particle), pointing in the y axis for the present choice of wave functions.

Actually the electric dipole can point in any direction (in general, perpendicular to traveling waves) at no cost of energy. To see this let us consider a phase rotation of the form (within $SU(3)$ rotations), $\psi^n \rightarrow \hat{\psi}^n$ with $(\psi^0, \psi^1, \psi^2) = (e^{-i\phi} \hat{\psi}^0, \hat{\psi}^1, e^{i\phi} \hat{\psi}^2)$. Note that $g_{\mathbf{p}}^{kn}$ are thereby transformed so that $\rho_{-\mathbf{p}}$ remains invariant. This transformation leaves $\mathcal{V} = V_X^{\text{DS}} + V_X^{\text{pz}}$ invariant; hence, the spectrum remains unchanged. Still the electric dipole thereby rotates so that

$$\mathbf{d} \equiv (d_x, d_y) = (\sin \phi, \cos \phi) |\mathbf{d}_e|. \quad (36)$$

It is now clear that a pair of solutions ψ and $Y\psi$, encountered earlier, differ by a rotation by π of coordinates in the sample plane.

V. GENERALIZATION

In this section we recover the electron spin and valley degrees of freedom and explore the PZM sector with both μ_Z and bias u , using the full Hamiltonian

$$H_{\text{eff}} = H_u + V_X^{\text{DS}} + V_X^{\text{pz}}. \quad (37)$$

We leave u arbitrary but keep $|u| \ll V_c$ so that one can still use the $u = 0$ expressions for $\mathcal{V} = V_X^{\text{DS}} + V_X^{\text{pz}}$, with u retained only in H_u as a small perturbation.⁴⁵

In addition, we ignore the difference between the intra- and interlayer Coulomb potentials that leads to a valley-symmetry breaking of $O(V_c d/\ell)$, with the layer separation $d \sim 0.35 \text{ nm} \ll \ell$. This breaking contains capacitance energies that determine how valleys rotate. In conventional bilayer systems, the capacitance energy, though as tiny as $O(V_c d^2/\ell^2)$, is positive and induces a valley rotation $(K, K') \rightarrow K \pm K'$, which makes the symmetric states $\propto K + K'$ lower in energy. In contrast, for bilayer graphene, capacitance energies turn out to be negative²⁴ and suppress possible valley rotations for $u \sim 0$.

Experimentally, it is difficult to directly observe valley quantum numbers, especially from the sequence in which

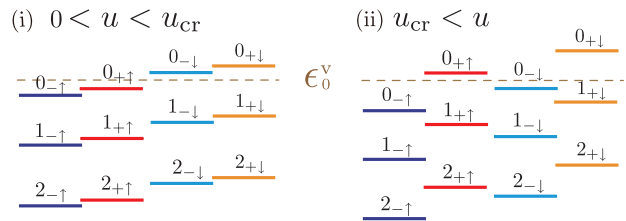


FIG. 2: Empty levels in the PZM sector at $\nu = -6$; for illustration, (i) $u = 0.25 u_{\text{cr}}$ and (ii) $u = 1.4 u_{\text{cr}}$ with $u_{\text{cr}} \equiv \mu_Z/(1 - z_2) \approx 1.2 \mu_Z$ and $\mu_Z/\tilde{V}_c = 0.05$.

the broken-symmetry states emerge with varying filling factor ν or magnetic field B . The sequence is governed by the Coulombic gaps, which, though possibly triggered by small valley or spin or orbital breaking, are practically insensitive in magnitude to small $|u| \ll V_c$. (In contrast, for large bias u , the valley is naturally polarized in either K or K' , depending on the sign of u .) For this reason, instead of a (rather laborious) analysis of capacitance energies, we here simply suppose a possible valley rotation $(K, K') \rightarrow (+, -)$ without specifying its details for small u ; we take the (-) state to be lower in energy for each $n \in (0, 1, 2)$ and spin $\alpha \in (\uparrow, \downarrow)$.

In H_{eff} the exchange interaction $V_X^{\text{DS}} + V_X^{\text{pz}}$ conserves both valley and spin, but breaks the orbital degeneracy. In contrast, the small perturbation H_u lifts all three degeneracies. Figure 2 depicts the empty PZM sector (at $\nu = -6$) governed by $H_u + V_X^{\text{DS}}$, with level spectra

$$\epsilon_n^{\pm\uparrow} = \epsilon_n^v \pm \epsilon_n^u - \frac{1}{2} \mu_Z, \quad \epsilon_n^{\pm\downarrow} = \epsilon_n^v \pm \epsilon_n^u + \frac{1}{2} \mu_Z, \quad (38)$$

in obvious notation. There are two possible level patterns, depending on (i) $0 \leq u < u_{\text{cr}}$ (of spin-breaking domination) or (ii) $u > u_{\text{cr}}$ (of valley-breaking domination) with $u_{\text{cr}} \equiv \mu_Z/(1 - z_2) [\approx 1.2 \mu_Z \text{ at } 10\text{T}]$. In Eq. (38), for definiteness, we have assumed no valley rotation and $u \geq 0$, so that $(+, -) = (K, K')$. When a valley rotation is induced (for small u), the $\pm \epsilon_n^u$ portions are replaced by more complex expressions, which, at any rate, are small for small u , and the level pattern (i) in Fig. 2 remains essentially intact. (For consistency, we set $u \rightarrow 0$ in our discussion for case (i) below.)

Let us start filling the empty PZM sector. Obviously, with $|u|, \mu_Z \ll V_c$, the orbital splitting among $\{\epsilon_n^v\}$ singles out the $2_{-\uparrow}$ level as the lowest-lying one in both cases (i) and (ii). It is thus the $2_{-\uparrow}$ level that is filled first. As it is being filled, it comes down in energy, followed by the $0_{-\uparrow}$ and $1_{-\uparrow}$ levels coupled via the exchange interaction V_X^{pz} . These three levels undergo orbital mixing, discussed in the previous section, through the $\nu = -5$ and -4 states until one reaches the $\nu = -3$ state, which is orbitally neutral (an $SU(3)$ singlet) but is polarized in valley and spin $(-, \uparrow)$. The associated $\nu = -3$ level gap is a valley gap for case (i) and a spin gap for case (ii),

$$\begin{aligned} \epsilon_{\nu=-3}^{\text{gap}}|_{(i)} &\approx 2 \epsilon_2^v, \\ \epsilon_{\nu=-3}^{\text{gap}}|_{(ii)} &= 2 \epsilon_2^v + \mu_Z, \end{aligned} \quad (39)$$

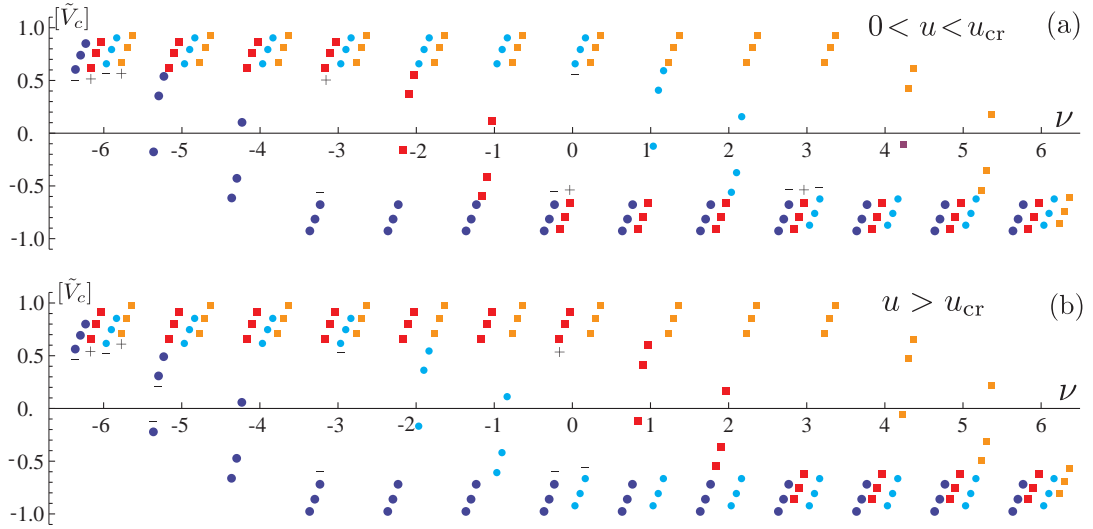


FIG. 3: Spectra of the PZM Landau levels at each integer filling factor $\nu \in [-6, 6]$. (a) $u = 0.4\mu_Z < u_{cr}$ and (b) $u = 2\mu_Z > u_{cr}$ with $\mu_Z/\tilde{V}_c = 0.05$ and $u_{cr} \equiv \mu_Z/(1 - z_2) \approx 1.2\mu_Z$ for illustration. Large blobs and squares refer to spin-up levels $(2_{-\uparrow}, 1_{-\uparrow}, 0_{-\uparrow})|_{\theta}$ and $(2_{+\uparrow}, 1_{+\uparrow}, 0_{+\uparrow})|_{\theta}$, respectively, from left to right; smaller symbols refer to those for the spin-down levels. Here $(2_{-\uparrow}, 1_{-\uparrow}, 0_{-\uparrow})|_{\theta}$, e.g., stands for $(2_{-\uparrow}, 1_{-\uparrow}, 0_{-\uparrow})$ for empty levels ($\theta = 0$) and $(0_{-\uparrow}, 1_{-\uparrow}, 2_{-\uparrow})$ for filled levels ($\theta = \pi/2$), in accordance with Fig. 1; empty levels have positive energy and occupied levels have negative energy. Valley indices \pm are attached to some symbols to indicate the nature of the associated gaps.

with $2\epsilon_2^v \approx 1.28\tilde{V}_c$. Similarly, as one goes up from $\nu = -3$ to $\nu = 0$, essentially the same orbital mixing is repeated for the $(+, \uparrow)$ sector in case (i) and for the $(-, \downarrow)$ sector in case (ii); analogously for the $\nu \in [0, 6]$ domain.

Figures 3 (a) and 3 (b) show the resulting spectra of the PZM multiplet at each integer filling factor $\nu \in [-6, 6]$. They differ in pattern for (i) $u \sim 0$ and (ii) $u > u_{cr}$, but form a perfectly particle-hole symmetric spectrum for the PZM sector in each case. The $\nu = \pm 2, \pm 1$ and 0 states thus differ in composition, depending on u . The $\nu = 0$ state, in particular, is spin-polarized for $u \sim 0$ and valley-polarized for $u > u_{cr}$, with a gap

$$\begin{aligned} \epsilon_{\nu=0}^{\text{gap}}|_{(i)} &\approx 2\epsilon_2^v + \mu_Z, \\ \epsilon_{\nu=0}^{\text{gap}}|_{(ii)} &= 2\epsilon_2^v + (1 - z_2)u - \mu_Z. \end{aligned} \quad (40)$$

As to the $\nu = -5$ gap, especially for case (ii) (of relatively large u), we note the following: $(\epsilon_0^u, \epsilon_1^u, \epsilon_2^u)$ in H_u , via the rotation \mathcal{U} , turns into $(0.96, 0.899, 0.897)u/2$, i.e., $\epsilon_1^u \approx \epsilon_2^u$ at $\nu = -5$; similarly, $\epsilon_0^u \approx \epsilon_1^u$ at $\nu = -4$. This suggests that the $\nu = (\pm 5, \pm 4, \pm 2, \pm 1)$ gaps are practically insensitive to both bias u and μ_Z , and equal to $\epsilon_{\nu=1,2}^{\text{gap}}$ in Eq. (33),

$$\epsilon_{\nu=\pm 5, \pm 4, \pm 2, \pm 1}^{\text{gap}} \approx 0.53\tilde{V}_c. \quad (41)$$

These orbital gaps are considerably smaller than the (Coulomb-enhanced $\nu = 0, \pm 3$) spin or valley gaps,

$$\epsilon_{\nu=\pm 1, \pm 2, \pm 4, \pm 5}^{\text{gap}} < \epsilon_{\nu=\pm 3}^{\text{gap}} \lesssim \epsilon_{\nu=0}^{\text{gap}} (\ll \epsilon_{\nu=\pm 6}^{\text{gap}}), \quad (42)$$

in conformity with Hund's rule.^{9,40} These $\nu = \pm 1, \pm 2, \dots$ orbital gaps and the $\nu = \pm 3$ valley gaps for $u \sim 0$ barely

depend on μ_Z and will therefore be insensitive to an additional parallel field B_{\parallel} in experiments with a tilted magnetic field, in contrast to the $\nu = 0$ spin gap for $u \sim 0$. For bilayer graphene, the corresponding gaps take place at $\nu = -3$ and -2 , and it was observed⁴⁶ that the associated resistance minima are barely affected by B_{\parallel} .

The orbitally polarized states at $\nu = \pm 1, \pm 2, \pm 4, \pm 5$ have spontaneous electric dipole moment and may potentially be unstable^{12,41,42} against charge inhomogeneities. Their spectra may be modified (in random patterns or regular^{41,42} patterns) around local charge concentrations but, as long as the orbital gaps survive, the quantum Hall states would emerge. Such an instability disappears when bias u is sufficiently large to stabilize the valley-polarized states. For bilayer graphene full splitting of the PZM levels has indeed been observed.^{46,47}

The transport properties of trilayers have been studied in a number of experiments.²⁶⁻³² Experimentally there is clear evidence for formation of the quantum Hall states in the basic filling-factor sequence $\nu = \pm 4(N + 3/2) = \pm 6, \pm 10, \pm 14, \dots$ for both *ABC*- and *ABA*-stacked trilayers. Evidence is yet very limited for the fine structure of the PZM sector with $|\nu| < 6$ in *ABC* trilayers: An experiment,³¹ using a Hall-bar device, observed a weak anomaly in σ_{xy} indicative of the developing $\nu = \pm 3$ gap. A clear signal for the $\nu = 0$ gap comes from the observation^{26,30} of the insulating state at the Dirac point ($\nu = 0$) in *ABC*-trilayer devices, both suspended and substrate-supported ones, with the resistance rising exponentially with increasing B and lowering temperature T . Experimentally, it is normally the $\nu = 0$ insulating state that is first observed as a nontrivial feature within the PZM sec-

tor of few-layer graphene. This suggests that the $\nu = 0$ gap is an interaction-enhanced gap rather than the far smaller intrinsic spin or valley gap. The $\nu = \pm 3$ gaps will be the next to be visible via quantized conductance. In view of Eqs. (39) and (40), the $\nu = 0$ gap will become even more prominent with increasing bias u , in contrast to the $\nu = \pm 3$ gap.

Finally we wish to discuss possible effects of nonleading interlayer couplings (v_4, v_3, γ_2). The effect of v_4 can be included in \mathcal{H}_n of Eq. (4) while v_3 and γ_2 induce transitions that go outside the PZM sector, as seen from the solutions in Eqs. (6) - (8). Accordingly the spectra ($\epsilon_0, \epsilon_1, \epsilon_2$) are corrected to first order in v_4/v and to second order in v_3/v and γ_2/γ_0 . With typical values^{28,43} $v_4/v \equiv r_4 \sim 0.01$, $v_3/v = \gamma_3/\gamma_0 \sim 0.1$, and $\gamma_2 \sim -0.02$ eV, such corrections are generally small. The leading $O(v_4)$ corrections, in particular, may conveniently be included in H_u if one sets $\epsilon_0^u = u/2$, $\epsilon_1^u = (1 - z_1)(u/2 + 2\kappa r_4 \omega_c)$ and $\epsilon_2^u = (1 - z_2)u/2 + 4\kappa(1 + \kappa^2)r_4 \omega_c$, with $2\kappa r_4 \sim 0.005$ and $4\kappa(1 + \kappa^2)r_4 \sim 0.01$. Unlike u , such $O(v_4)$ corrections are common to the K and K' valleys and lead to weak electron-hole asymmetry. The relative magnitude of ($\epsilon_0^u, \epsilon_1^u, \epsilon_2^u$) may vary with bias u and can potentially control a valley rotation for small $u \sim 0$. Still the orbital splitting among $\{\epsilon_n^v\}$ is generally larger than the splitting among $\{\epsilon_n^u\}$, and the PZM sector will essentially maintain the spectra shown in Fig. 3. The electron-hole symmetric spectra there will also serve as the base point for further examining possible effects of nonleading intra- and interlayer parameters.

VI. SUMMARY AND DISCUSSION

In a magnetic field graphene trilayers acquire, on topological grounds, a special multiplet of nearly-zero-energy Landau levels with a threefold degeneracy in Landau orbitals. In this paper we have studied the structure of this PZM multiplet in ABC -stacked trilayer graphene and pointed out that its orbital degeneracy is lifted by quantum fluctuations of the valence band. Here we encounter a trilayer generalization of the ‘‘orbital’’ Lamb shift, discussed earlier for bilayer graphene. The splitting among the shifted energies $\{\epsilon_n^v\}$ acts as a quantum orbital breaking that generally exceeds intrinsic spin or valley breaking in scale, and essentially governs the structure of the PZM sector.

The orbital Lamb shift of the PZM Landau levels is a ‘‘field-theoretic’’ vacuum effect but is intimately correlated with the Coulomb interaction acting within the multiplet. This is because they have to combine to yield an electron-hole symmetric spectrum for the PZM multiplet (with only the leading couplings γ_0 and γ_1 kept) as a whole. In particular, large Coulombic gaps, expected at $\nu = 0$ and ± 3 , are essentially given by the energy scale $\sim 2e_v^2$ of the orbital Lamb shift.

The PZM levels get mixed via the Coulomb interaction and avoid level crossing, keeping smaller orbital gaps (of magnitude $\sim 0.5\tilde{V}_c$), as we have seen in Sec. V. Level crossing, if present, would enhance the degree of degeneracy and the steps of Hall plateaus would jump accordingly. Observations of possible $\nu = \pm 1, \pm 2, \pm 4, \pm 5$ quantum Hall states in high-quality samples, such as suspended or BN-supported ones, under high magnetic fields, if achieved, would be direct evidence for the presence of orbital mixing without level crossing. It is also possible, in principle, to detect the orbital gaps via cyclotron resonance within the PZM sector.^{9,24}

In this paper we have focused on ABC -stacked trilayer graphene. We remark that our analysis and conclusion cannot simply be carried over to the case of ABA trilayers, which lacks a direct link between the K - and K' -valley expressions [such as Eq. (2)] and which thus requires a separate analysis.⁴⁸

Acknowledgments

This work was supported in part by a Grant-in-Aid for Scientific Research from the Ministry of Education, Science, Sports and Culture of Japan (Grant No. 24540270).

Appendix A: Derivation of Eq. (21)

In this appendix we present a proof of the completeness relation $\sum_n |g_{\mathbf{p}}^{kn}|^2 = e^{\ell^2 \mathbf{p}^2/2}$ in Eq. (21). A simpler version of it is the following:

$$\sum_{n=0}^{\infty} \int_{\mathbf{p}} f_{\mathbf{p}}^{kn} f_{-\mathbf{p}}^{nm} = e^{\ell^2 \mathbf{p}^2/2} \delta^{km} \quad (\text{A1})$$

for integers $k, m \geq 0$, which is verified by use of the explicit form of $f_{\mathbf{p}}^{kn}$ in Eq. (14). We show that Eq. (21) is essentially reduced to Eq. (A1).

Let us first look at Eq. (13) and put the (orthonormal set of) six eigenvectors of \mathcal{H}_n for each $n \in (3, 4, \dots)$ into the orthogonal matrix $T_n = (\mathbf{v}_{n_1}, \mathbf{v}_{n_2}, \dots, \mathbf{v}_{n_6})$ with $|n_\sigma| = n$ and $\sigma \in (1, 2, \dots, 6)$. The first row of T_n is $(b_{n_1}^{(1)}, b_{n_2}^{(1)}, \dots, b_{n_6}^{(1)}) \equiv \{b_{n_\sigma}^{(1)}\}$, the second row is $\{d_{n_\sigma}^{(1)}\}$, etc. These row vectors also form an orthonormal basis. This feature is also true for $n \in (0, 1, 2)$, except that T_n has a smaller rank.

In taking the product $\sum_n g_{\mathbf{p}}^{kn} g_{-\mathbf{p}}^{nm}$ one may first sum over n_σ for each fixed $n = |n_\sigma|$. One thereby encounters inner products of the row vectors such as $\sum_\sigma \{b_{n_\sigma}^{(i)}\} \{b_{n_\sigma}^{(j)}\} = \delta^{ij}$ and $\sum_\sigma \{b_{n_\sigma}^{(i)}\} \{d_{n_\sigma}^{(j)}\} = 0$. The remaining sum over $|n|$ is essentially reduced to formula (A1) and one eventually finds that $\sum_n g_{\mathbf{p}}^{kn} g_{-\mathbf{p}}^{nm} = e^{\ell^2 \mathbf{p}^2/2} \delta^{|k|, |m|} (\mathbf{v}_k \cdot \mathbf{v}_m)$, which leads to Eq. (21).

-
- ¹ K. S. Novoselov, A. K. Geim, S. V. Morozov, D. Jiang, M. I. Katsnelson, I. V. Grigorieva, S. V. Dubonos, and A. A. Firsov, *Nature (London)* **438**, 197 (2005).
- ² Y. Zhang, Y.-W. Tan, H. L. Stormer, and P. Kim, *Nature (London)* **438**, 201 (2005).
- ³ Y. Zheng and T. Ando, *Phys. Rev. B* **65**, 245420 (2002).
- ⁴ E. McCann and V. I. Fal'ko, *Phys. Rev. Lett.* **96**, 086805 (2006).
- ⁵ T. Ohta, A. Bostwick, T. Seyller, K. Horn, and E. Rotenberg, *Science* **313**, 951 (2006).
- ⁶ E. McCann, *Phys. Rev. B* **74**, 161403(R) (2006).
- ⁷ E. V. Castro, K. S. Novoselov, S. V. Morozov, N. M. R. Peres, J. M. B. Lopes dos Santos, J. Nilsson, F. Guinea, A. K. Geim, and A. H. Castro Neto, *Phys. Rev. Lett.* **99**, 216802 (2007).
- ⁸ A. J. Niemi and G. W. Semenoff, *Phys. Rev. Lett.* **51**, 2077 (1983).
- ⁹ Y. Barlas, R. Côté, K. Nomura, and A. H. MacDonald, *Phys. Rev. Lett.* **101**, 097601 (2008).
- ¹⁰ R. Nandkishore and L. Levitov, *Phys. Rev. B* **82**, 115124 (2010).
- ¹¹ E. V. Gorbar, V. P. Gusynin, Junji Jia, and V. A. Miransky, *Phys. Rev. B* **84**, 235449 (2011).
- ¹² K. Shizuya, *Phys. Rev. B* **79**, 165402 (2009).
- ¹³ Y. Barlas, R. Côté, J. Lambert, and A. H. MacDonald, *Phys. Rev. Lett.* **104**, 096802 (2010).
- ¹⁴ R. Côté, J. Lambert, Y. Barlas, and A. H. MacDonald, *Phys. Rev. B* **82**, 035445 (2010).
- ¹⁵ R. Côté, W. Luo, B. Petrov, Y. Barlas, and A. H. MacDonald, *Phys. Rev. B* **82**, 245307 (2010).
- ¹⁶ R. Côté, J. P. Fouquet, and W. Luo, *Phys. Rev. B* **84**, 235301 (2011).
- ¹⁷ J. González, F. Guinea, and M. A. H. Vozmediano, *Nucl. Phys. B* **424**, 595 (1994).
- ¹⁸ T. Misumi and K. Shizuya, *Phys. Rev. B* **77**, 195423 (2008); K. Shizuya, *Phys. Rev. B* **75**, 245417 (2007).
- ¹⁹ Z. Jiang, E. A. Henriksen, L. C. Tung, Y.-J. Wang, M. E. Schwartz, M. Y. Han, P. Kim, and H. L. Stormer, *Phys. Rev. Lett.* **98**, 197403 (2007).
- ²⁰ A. Iyengar, J. Wang, H. A. Fertig, and L. Brey, *Phys. Rev. B* **75**, 125430 (2007).
- ²¹ Yu. A. Bychkov and G. Martinez, *Phys. Rev. B* **77**, 125417 (2008).
- ²² S. Viola Kusminskiy, D. K. Campbell, and A. H. Castro Neto, *Europhys. Lett.* **85**, 58005 (2009).
- ²³ K. Shizuya, *Phys. Rev. B* **81**, 075407 (2010); *Phys. Rev. B* **84**, 075409 (2011).
- ²⁴ K. Shizuya, *Phys. Rev. B* **86**, 045431 (2012).
- ²⁵ W. E. Lamb and R. C. Retherford, *Phys. Rev.* **72**, 241 (1947). See also, C. Itzykson and J.-B. Zuber, *Quantum field theory*, (McGraw-Hill, New York, 1980).
- ²⁶ W. Bao, Z. Zhao, H. Zhang, G. Liu, P. Kratz, L. Jing, J. Velasco, Jr., D. Smirnov, and C. N. Lau, *Phys. Rev. Lett.* **105**, 246601 (2010).
- ²⁷ A. Kumar, W. Escoffier, J. M. Pumirol, C. Faugeras, D. P. Arovas, M. M. Fogler, F. Guinea, S. Roche, M. Goiran, and B. Raquet, *Phys. Rev. Lett.* **107**, 126806 (2011).
- ²⁸ T. Taychatanapat, K. Watanabe, T. Taniguchi, and P. Jarillo-Herrero, *Nat. Phys.* **7**, 621 (2011).
- ²⁹ C. H. Lui, Z. Li, K. F. Mak, E. Cappelluti, and T. F. Heinz, *Nat. Phys.* **7**, 944 (2011).
- ³⁰ W. Bao, L. Jing, J. Velasco Jr, Y. Lee, G. Liu, D. Tran, B. Standley, M. Aykol, S. B. Cronin, D. Smirnov, M. Koshino, E. McCann, M. Bockrath, and C. N. Lau, *Nat. Phys.* **7**, 948 (2011).
- ³¹ L. Zhang, Y. Zhang, J. Camacho, M. Khodas, and I. Zaloznyak, *Nat. Phys.* **7**, 953 (2011).
- ³² S. H. Jhang, M. F. Craciun, S. Schmidmeier, S. Tokumitsu, S. Russo, M. Yamamoto, Y. Skourski, J. Wosnitza, S. Tarucha, J. Eroms, and C. Strunk, *Phys. Rev. B* **84**, 161408(R) (2011).
- ³³ F. Guinea, A. H. Castro Neto, and N. M. R. Peres, *Phys. Rev. B* **73**, 245426 (2006).
- ³⁴ M. Koshino and T. Ando, *Phys. Rev. B* **76**, 085425 (2007).
- ³⁵ J. Nilsson, A. H. Castro Neto, F. Guinea, and N. M. R. Peres, *Phys. Rev. B* **78**, 045405 (2008).
- ³⁶ M. Koshino and E. McCann, *Phys. Rev. B* **80**, 165409 (2009).
- ³⁷ M. Koshino and E. McCann, *Phys. Rev. B* **81**, 115315 (2010).
- ³⁸ F. Zhang, B. Sahu, H. Min, and A. H. MacDonald, *Phys. Rev. B* **82**, 035409 (2010).
- ³⁹ S. Yuan, R. Roldan and M. I. Katsnelson, *Phys. Rev. B* **84**, 125455 (2011).
- ⁴⁰ F. Zhang, D. Tilahun, and A. H. MacDonald, *Phys. Rev. B* **85**, 165139 (2012).
- ⁴¹ Y. Barlas, R. Côté, and M. Rondeau, *Phys. Rev. Lett.* **109**, 126804 (2012).
- ⁴² R. Côté, M. Rondeau, Anne-Marie Gagnon, and Y. Barlas, *Phys. Rev. B* **86**, 125422 (2012).
- ⁴³ L. M. Zhang, Z. Q. Li, D. N. Basov, and M. M. Fogler, Z. Hao, and M. C. Martin, *Phys. Rev. B* **78**, 235408 (2008).
- ⁴⁴ For $n \in (0, 1, 2)$, $b_n^{(i)}$ are odd in u while $d_n^{(i)}$ are even in u ; also z_1 and z_2 are functions of $(\hat{u}, \hat{\gamma}^2)$.
- ⁴⁵ For large bias $|u| \gtrsim V_c$ one needs to improve the orbital rotation \mathcal{U} along with the improved $\{\epsilon_n^v\}$.
- ⁴⁶ Y. Zhao, P. Cadden-Zimansky, Z. Jiang, and P. Kim, *Phys. Rev. Lett.* **104**, 066801 (2010).
- ⁴⁷ B. E. Feldman, J. Martin, and A. Yacoby, *Nat. Phys.* **5**, 889 (2009); R. T. Weitz, M. T. Allen, B. E. Feldman, J. Martin, and A. Yacoby, *Science* **330**, 812 (2010).
- ⁴⁸ A preliminary look into *ABA* trilayers reveals that the orbital Lamb shift significantly differs between the *K* and *K'* valleys.